43rd AIAA/ASME/SAE/ASEE Joint Propulsion Conference & Exhibit
8 - 11 July 2007, Cincinnati, OH

AIAA 2007-5638

Time- Dependent Nozzle Erosion Process in a Solid Propellant Rocket Motor

Nicholas D. Liggett[1] and Suresh Menon[2]
The Georgia Institute of Technology, Atlanta, GA 30332-0150

This paper presents an approach to simulate erosion of rocket nozzle wall using a physics based model that relies on as little empirical data as possible. A model is developed from basic conservation equations taking into account conservation of species, momentum, and energy in Lagrangian framework applied in a lattice-based simulation model. The Mie-Grüneisen equation of state is also included to allow the propagation of shockwaves and detonation into reactive materials. Various studies have been conducted to validate this model. Past studies focused on surface erosion of the nozzle due to shear forces, heat transfer, and surface chemistry. In the current study, the model is applied to the regression of a sandwich propellant consisting of ammonium perchlorate with a polybutadiene binder to demonstrate its usefulness in modeling surface regression during burning of composite solid rocket fuel. Additionally, a three-dimensional study of particle impact on material to investigate surface cratering that might occur on nozzle walls.

I. Introduction

THE erosion of the walls of a solid rocket nozzle is caused by various physical factors. Most notable factors among them are erosion due to thermo-fluid effects such as heat transfer to the walls, shear and normal stresses on the wall due to the fluid boundary layer, temperature, pressure, surface kinetics and particles impinging on the nozzle walls.[1] These effects are shown in Fig. 1. The erosion near or at the nozzle wall is of particular interest here since the throat of a solid propellant rocket nozzle is subject to extreme conditions.[2] It is the region of the highest heat transfer, and this extreme heat transfer along with surface shear forces and impact of particulates in the flow can lead to surface erosion of the nozzle. Two failure modes might occur. Either the rocket might fail catastrophically as the throat weakens, or the throat might grow to the point where the flow is no longer choked. Either case is undesirable, and therefore understanding of throat erosion is critical to design. Additionally, to increase the performance of rockets, it is desirable to increase the chamber pressure. This increase leads to even more intense conditions at the throat. A fundamental understanding of the underlying processes is not currently available since it is nearly impossible to fully resolve the processes occurring near the wall. Current erosion prediction methods are either highly specific or lacking many aspects of the nozzle erosion process.[3-9] As such, the need for better understanding of throat erosion from a more fundamental viewpoint and its sensitivity to chamber operating conditions is even more apparent.

The current study is focused on developing a comprehensive simulation strategy that can capture not only the local thermo-chemical processes impacting nozzle erosion, but also the geometrical changes to the nozzle surface. To accomplish this we need a simulation approach that includes both the physics of the processes and the ability to capture the changes to the geometry of the nozzle surface in response to these processes. An added difficulty is that the heat transfer, chemistry, and mechanical time scales of erosion are all very different creating a stiff system to solve. These fine-scale physics have to be captured within a simulation framework that also resolves the gas phase combustion physics that constitute the prescribed rocket combustion conditions under which the erosion takes place.

Current erosion simulation strategies focus one only one or two aspects of the erosion process or they cannot be generalized to suit the needs of nozzle erosion. Much erosion work has been devoted to the prediction of gun barrel erosion;[3,4] however, this work is highly specific to gun barrel erosion and difficult to apply to rocket motor nozzle erosion. Another erosion model that is designed to simulate erosion due to dilute particle impacts[5,6] agrees well with

[1] Graduate Research Assistant, Computational Combustion Laboratory, School of Aerospace Engineering; Nicholas.Liggett@mail.gatech.edu. Member AIAA.
[2] Professor, Director, Computational Combustion Laboratory, School of Aerospace Engineering; suresh.menon@ae.gatech.edu. Associate Fellow AIAA.

experiments, but it contains only the effects of particle impacts and is not easily extended to include all erosive effects along with a moving wall boundary. It also relies on knowing empirical parameters, such as the area of contact between the particles and the boundary, which may not be known a priori for high speed impacting particles, which can deform and break apart upon impact. Erosion models that are specifically tailored to predict erosion in a solid rocket motor due to alumina particles also exist.[7] This model also includes the effects of heat transfer to the surface. Unfortunately it does not fully account for surface kinetics and relies on empirical parameters for the particle impact model, restricting its use. Finally, models that are focused on ablation of protective linings[8,9] sufficiently account for heat transfer, but they lump together all chemistry that occurs at the surface or rely on correlative equations, so that understanding the workings of the various aspects of erosion is difficult.

This study aims to create a comprehensive erosion model that can account for all aspects of the erosion process within a rocket nozzle. We seek to create an erosion model that does not depend on empirical correlations and the model is expected to have wide applicability not only to nozzle erosion, but also to solid propellant combustion and impact modeling.

Simulations of particle impacts into a solid surface have many applications. In rocket motors, metalized propellants can produce metal particles that are ejected into the gas flow. The model to capture this particle impact is an extended macro-scale dynamic (MSD) model, which has been developed and validated by other authors.[10-12] This model is specifically designed to model erosion due to these particle impacts. It is based on first principles of Newton's laws of motion applied on a discrete lattice representing the surface, and as such is applicable to almost any situation involving particle impacts. Additionally, this model already satisfies the conservation of momentum requirement through a Lagrangian approach. This approach provides an excellent framework, in that it is extensible (properties can be added to the lattice points as desired) and allows materials that are nonuniform in composition and even composite materials to be analyzed.[13] Additionally, the model allows simulation at the scale at which erosion takes places without being prohibitively slow for computations, as an atomic model would be. However, the original MSD model has some well known deficiencies that must be corrected for general application of current interest. This paper addresses these issues.

Our previous work[1,14] extended this macro-scale dynamical model to include heat transfer and surface force effects. In the current study the model has been further extended to include chemical kinetics and full coupling between all different erosion aspects. The erosion model that is developed includes the effects of pressure and shear forces from the hot gases. Heat transfer effects are also included, as they are known to lead to melting of the material and thus erosion of the nozzle.[9] A numerical heat transfer model[15,16] is modified to fit into the framework of the MSD model. Although it is not included in this study, the effect of thermal expansion can be added. Heat transfer leads not only to melting of the material, but the increase in temperature weakens the nozzle mechanically and increases the reaction rates of heterogeneous reactions occurring at the nozzle surface.[17] These heterogeneous reactions are another source of nozzle erosion that is included in the study, as they can be a significant source of erosion in carbon nozzles.[18]

II. Model Formulation

In order to create a high fidelity erosion model capable of diverse applications, one must begin at the basic conservation laws applied to the system consisting of the nozzle wall. A Lagrangian approach is taken with the system being an open system with a control volume that is unsteady. This control volume surrounds all the solidified mass of the wall, but does not surround the reacting mass that leaves via heterogeneous surface reactions. In other words, the mass that is taken up by heterogeneous reactions is considered mass that exits the system through the control surface. Note that *condensed* mass ejected due to particle impacts or other means is still considered part of the system, but the control volume then takes up a disconnected shape to encircle all solid mass and not encircling the mass lost as gas. There is no mass inlet to our system. Additionally, the only mass exit is through the heterogeneous chemical reactions that occur at the surface. At the control surface, boundary conditions are applied that are obtained either from a flow field solver or through some other understanding of the physical system. For example, a nozzle wall might have an applied heat flux from the hot gases on one portion of the control surface and a perfectly insulated condition on another portion of the control surface.

A. Conservation Equations

All species must be conserved, that is the change in concentration of a chemical species must be balanced by mass transfer of the chemical species through the control surface of the system due to convection and diffusion along with chemical reaction sources and sinks. In our system there is no convection of mass across the control surface, as the control volume constantly contains all mass of the system, with the exception of that lost due to

heterogeneous reactions. Additionally, any solid-solid mass diffusion across the control surface is neglected in light of the short firing times of the rocket. This leaves only the chemical reactions as a source/sink for species conservation. Condensed phase chemical reactions are not considered here. The composition of the interior portion of the condensed phased is considered constant. We are considering heterogeneous reactions that only remove mass from the wall, so that they do not deposit mass to the wall. Additionally, any particle collisions are assumed not to add mass to the system. Their mass is kept separate from the wall system, with their own sets of conservation equations being solved, and the interaction effects between the systems being handled through boundary conditions.

The conservation equation for chemical species that must be satisfied for each species considered for the nozzle wall is:

$$\frac{d}{dt}\int_V \rho_k dV = \int_S \dot{\omega}_k dS \tag{1}$$

Here, $\dot{\omega}_k$ is the reaction rate of the conserved species k in units of a mass flux, ρ_k is the density of the conserved species, and t is the time. The left hand integral is over the control volume V, whereas the right hand integral is over the associated control surface S. For the control surface boundary in contact with the hot gases, the reaction rate value is given by the appropriate reaction rates as determined by the local species concentrations and temperature. In our current study, these kinetics are modeled using modified Arrhenius rate equations of the form $k = AT^{\eta}\exp[E_A/(RT)]$, where A, η, and E_A are empirical constants that are different for each reaction of the mechanism. For the solid-solid boundary the reaction rate is zero, leading to a constant interior condensed phase composition. Note molecular diffusion is neglected in this formulation, as the characteristic times over which it occurs are large in comparison to the characteristic times for rocket nozzle erosion.

The conservation of mass for our open system is:

$$\frac{d}{dt}\int_V \rho dV = \dot{m} = \int_S \sum_{\text{all species}} [\dot{\omega}_k] dS \tag{2}$$

Here, ρ is the mixture density, the mass fraction weighted average of the species densities ρ_k. This conservation equation is the summation of all the individual species conservation equations, so that it is identically satisfied if all species conservation equations are individually satisfied. The entire desired chemical reaction mechanism is explicitly seen here. This equation states that the rate of change of the mass of the wall and any of its ejected pieces is equation to the mass flux integrated over the wall surface exposed to the reacting fluid. Note that the change in mass of the system over time is may not be zero due to mass exiting the system through surface chemical kinetics.

The conservation of momentum is the next conservation equation considered. This conservation law is derived from Newton's second law:

$$m \cdot \vec{a} = \vec{F} \tag{3}$$

The mass times the acceleration vector on the left-hand side is the change in the total momentum within the control volume over time. The right-hand side is the total force acting on the control volume, including all surface and body forces. Currently, no body forces are considered, so that this force term should be the integrated effect of all surface forces. For our Lagrangian approach, the control surface constantly encircles the same mass, so that no convection of momentum across the surface can occur. Momentum carried with mass that is lost due to chemical reactions at the control surface is neglected. The resulting integral momentum equation is:

$$\frac{d}{dt}\int_V \rho \vec{u} dV = \int_S \bar{\bar{\sigma}} \cdot d\vec{S} \tag{4}$$

Here, $\vec{u}$ is the velocity of the condensed phase material and $\bar{\bar{\sigma}}$ is the surface stress tensor representing all the surface forces to be defined.

The conservation of energy law is:

$$\frac{d}{dt}\int_V \rho\left(e+\frac{|\vec{u}|^2}{2}\right)dV = \int_S (q''_{\text{conv}}+q''_{\text{rad}})dS + \int_S k\vec{\nabla}T\cdot d\vec{S} + \int_S \vec{\nabla}\cdot(\bar{\bar{\sigma}}\cdot\vec{u})\,d\vec{S} + \int_S \sum_{\text{all species}} [\dot{\omega}_k h_k]\,dS \tag{5}$$

Here, e is the specific internal energy per unit mass, q''_{conv} is the heat flux due to convection across the control surface, q''_{rad} is the heat flux due to radiation across the control surface, k is the thermal conductivity of the condensed phase, and h_k is the specific enthalpy per unit mass of the condensed phase.

The total energy per unit mass is comprised of the specific internal energy and the kinetic energy. The first integral on the right-hand side is the total heat flux integral comprised of the convective and radiative heat fluxes with the hot gases and the conductive heat flux with the rest of the condensed phase in contact with the control surface. The radiative heat flux should take into account the incident radiation from the hot gases and the emitted radiation from the wall surface. The conductive heat flux is obtained from the Fourier law of conduction. The second integral is the total work performed on the control volume at the control surface. At the control surface in contact with the eroding gases, the work is done by the normal pressure and shear stress of the gases. At the control surface in contact with the rest of the condensed phase, the work is done by the pressure of the condensed phase and the mechanical normal and shear stresses. The last integral is the heat released by the heterogeneous chemical reactions at the control surface.

B. Constitutive Relations

The surface stress tensor is defined to include all surface forces acting on the control volume. The surface forces are divided between normal and shear forces from the surrounding fluid at the eroding control surface, and normal and shear mechanical stresses due to strains with the surrounding condensed phase. Additionally, there is a normal pressure originating from the surrounding condensed phase. All these stresses are contained within the stress tensor, and are integrated over the respective region of the control surface to obtain the total force on the control volume. The shear and normal pressures due to the hot eroding gases are determined from a coupled fluid solver. The fluid solver solution serves as the boundary condition for the control surface.

The surface stress tensor for the control surface is:

$$\bar{\bar{\sigma}} = \begin{pmatrix} -p_{\text{surf}}-\theta_{11} & \tau_{12}+\theta_{12} & \tau_{13}+\theta_{13} \\ \tau_{21}+\theta_{21} & -p_{\text{surf}}-\theta_{22} & \tau_{23}+\theta_{23} \\ \tau_{31}+\theta_{31} & \tau_{32}+\theta_{32} & -p_{\text{surf}}-\theta_{33} \end{pmatrix} \tag{6}$$

Here, if the control surface is in contact with the hot eroding gases, p_{surf} is the normal gas pressure p_{gas} of the fluid, the off-diagonal τ_{ij} are the shear pressures between the gas and wall, and the mechanical stresses θ_{ij} are all zero. If the control surface is in contact with the rest of the condensed phase, p_{surf} is the normal condensed phase pressure p_{solid}, given by the equation of state for the condensed phase, the gas shear pressures τ_{ij} are zero. The diagonal mechanical normal stresses θ_{ii} and remaining off-diagonal mechanical shear stresses θ_{ij} are given by stress-strain relationships for the condensed phase.

At this point a model for the stresses must be implemented. Stress-strain relationships can be utilized to model the strain at the wall surface as separate elastic and plastic components with associated stresses. The strains are converted to stresses using Hooke's law in three dimensions:

$$\varepsilon_1 = \frac{1}{E}\left[\theta_{11} - \nu\left(\theta_{22}+\theta_{33}\right)\right] + \alpha\cdot T \tag{7a}$$

$$\varepsilon_2 = \frac{1}{E}\left[\theta_{22} - \nu\left(\theta_{11}+\theta_{33}\right)\right] + \alpha\cdot T \tag{7b}$$

$$\varepsilon_3 = \frac{1}{E}\left[\theta_{33} - \nu\left(\theta_{11} + \theta_{22}\right)\right] + \alpha \cdot T \tag{7c}$$

Here, ε_i is normal strain of the wall referenced to its undeformed state, E is the plastic or elastic modulus, depending on the strain state, and ν is Poisson's ratio. The thermal expansion coefficient and temperature are α and T, respectively, included to model the mechanical effects of temperature gradients in the material.

The shear strains, γ_{ij}, of the control surface are converted to shear stresses through the shear modulus, G:

$$\gamma_{12} = \frac{\theta_{12}}{G} = \frac{\theta_{21}}{G} \tag{8a}$$

$$\gamma_{23} = \frac{\theta_{23}}{G} = \frac{\theta_{32}}{G} \tag{8b}$$

$$\gamma_{13} = \frac{\theta_{13}}{G} = \frac{\theta_{31}}{G} \tag{8c}$$

The strain state of the control surface is calculated using the MSD model to be discussed. The MSD model gives the undeformed reference state. The strains are then substituted into Eqns. 7 and 8 to obtain the stress state, which is then substituted into the stress tensor.

To close these equations an equation of state is needed. The exact for depends on the problem in question. For the solid material we include an equation of state in the Mie-Grüneisen form. This form of the equation of state has been validated for shockwave propagation through inert and reactive materials.[32] The specific internal energy of the wall is given by Rankine-Hugoniot relations with a pressure energy addition:

$$e(p, \nu) = e_H(\nu) + \frac{\nu}{\Gamma} \cdot \left[p - p_H(\nu)\right] \tag{9}$$

Here, ν is the specific volume of the condensed phase and Γ is the Grüneisen gamma. For inert materials, $e_H(\nu)$ and $p_H(\nu)$ are given by the shock Rankine-Hugoniot relations as:

$$e_H(\nu) = \frac{1}{2}\, p_H(\nu) \cdot (\nu_0 - \nu) \tag{10}$$

$$p_H(\nu) = c_0^2\, \frac{(\nu_0 - \nu)}{\left[\nu_0 - s \cdot (\nu_0 - \nu)\right]} \tag{11}$$

Here, c_0 is the ambient speed of sound, ν_0 is the ambient specific volume, and s is the slope of the linear shock Hugoniot. A commonly used assumption for inert materials is:

$$\frac{\nu}{\Gamma} = \frac{\nu_0}{\Gamma_0} \tag{12}$$

Here, Γ_0 is the ambient Grüneisen gamma. For reactive materials, the relations for the Hugoniot energy and pressure will be more complex depending on the problem specific mixture of reactants and products.

C. Computational Methods

The full set of conservation equations consisting of Eqns. 1, 4, and 5 and the constitutive relations consisting of equations 6 and 9 form a system of equations that will give the solution to the nozzle erosion problem. These

equations are a complex system for which an analytical solution is currently not known. A Lagrangian computational model based on the MSD approach is applied here.

The nozzle wall is first discretized into *N* Lagrangian non-overlapping control volumes. Some control volumes are boundary control volumes in contact with the global control surface, whereas some are interior control volumes being completely surrounding by the wall condensed phase. The conservation equations are solved in all these control volumes. The properties of the control volume, i.e. density, temperature, velocity, etc., are stored at the central point ***P*** of the control volume cells. The conservation equations are then written for each of the control volumes as seen below.

$$\frac{d}{dt}\left(\rho_k V\right) = \sum_{j=1}^{n_f} \int_{A_j} \dot{\omega}_k dA_j \tag{13}$$

$$\frac{d}{dt}(\rho \vec{u} V) = \sum_{j=1}^{n_f} \int_{A_j} \bar{\bar{\sigma}} \cdot d\vec{A}_j \tag{14}$$

$$\frac{d}{dt}\left[\rho\left(e + \frac{|\vec{u}|^2}{2}\right)V\right] = \sum_{j=1}^{n_f} \int_{A_j} \left(q''_{\text{conv}} + q''_{\text{rad}} + \sum_{\text{all species}} [\dot{\omega}_k h_k]\right) dA_j + \sum_{j=1}^{n_f} \int_{A_j} \left[k\vec{\nabla}T + \bar{\bar{\nabla}} \cdot (\bar{\bar{\sigma}} \cdot \vec{u})\right] \cdot d\vec{A}_j \tag{15}$$

The surface integrals are broken into summations of integrals over each of the n_f faces of the discretized control volume. The properties of the material that are needed for the integrals at the surface of the discretized control volume are found by utilizing a linear distribution of the values between the local computational points. The time derivative is solved by a finite-differencing fully explicit scheme.

In the MSD model, the target material and the impacting particle(s) (if applicable) are discretized onto a lattice. Each site of the lattice represents a small fictitious volume of the material. In our formulation, the lattice site is the computational point at the center of the control volume. During the erosion process, any lattice site is vulnerable to movement due to the action of the external forces caused by various processes such as surface chemistry, surface shear and normal loads, as well as due to interactions between any pair of adjacent sites. Each pair of adjacent sites is linked by an imaginary "bond." This bond should not be mistaken for a molecular bond between a pair of atoms, but as a hypothetical bond for the purpose of modeling. The deformation of this imaginary bond is responsible for the interactions between any pair of adjacent sites. This deformation is, in turn, dependent on the mechanical properties of the material. Any bond between two adjacent sites will break if the mechanical strain caused in the bond due to its deformation exceeds the fracture strain of the material. Any site or a group of sites is liable to be eroded away if all the bonds surrounding it are broken due to fracture.

The MSD model is implemented within a finite volume approach that is well suited to a grid in which pieces are removed by erosion. An interior site of the nozzle wall is seen in Fig. 2a. The springs represent the forces between the site and its neighboring sites. Heat transfer also occurs along these springs. The state and change in state of an interior node is dependent upon only the initial conditions and its neighboring nodes; however, for an exterior node, boundary conditions such as prescribed heat transfer or temperature are applied. An example of an exterior site is shown in Fig. 2b, where the bond between node and its top neighbor does not exist, so that no conductive heat or force transfer can occur. At this surface site, shear forces can be seen that are dependent on the shear stress at the surface. There will also be pressure forces that are not shown for clarity. Finally, this surface site will have mass loss from its point mass load due to chemical kinetics. If this surface site is removed by erosion the site below it will become a surface node.

These nodes represent the discretized control volumes for which each of the conservation equations, Eqs. 14, 15, and 16, are solved. The control volumes, or nodes, can be removed from the material for several reasons. A site will be eroded and removed from the material matrix if it reaches the melting temperature of the material. If all control surface connections, or springs, are broken, the control volume is free to be entrained into the hot gas flow. Finally,

if all the mass of a control volume is used up in heterogeneous reactions, the control volume site is no longer considered in calculations.

The springs of the nodes are the contact points between the control surfaces of neighboring control volumes. The start of the simulation is considered the undeformed state of the control volume. The deformation vector of the bond between any two adjacent sites ***P*** and ***Q*** is given by:

$$\Delta\vec{r}(P,Q) = \vec{r}(P,Q) - \vec{r}_0(P,Q) = \left[\vec{r}(Q) - \vec{r}(P)\right] - \vec{r}_0(P,Q) \tag{16}$$

Here, $\vec{r}(P,Q)$ is the relative position vector between nodes ***P*** and ***Q*** and $\vec{r}(P)$ is the absolute position vector of node ***P***. The subscript 0 denotes the initial undeformed state of the material. The normal strain ε for a control surface between two ajacent sites is then given by the magnitude of the deformation vector. The shear strain for a control surface is given by:

$$\gamma = \arccos\left[\frac{\Delta\vec{r}(P,Q)\cdot\vec{r}(P,Q)}{\left\|\Delta\vec{r}(P,Q)\right\|\left\|\vec{r}(P,Q)\right\|}\right] \tag{16}$$

These normal and shear strains are converted to stresses using the rheological model shown in Fig. 3 along with the three-dimensional stress-strain relationships from Eqns. 7 and 8. The stress-strain rheological model consists of sliders and springs modeling a linear elastic portion and any number of piecewise linear plastic portions of a desired stress-strain curve.

Finally, with the conservation equations integrated, the location of the control volumes must be updated. The position of the site at a time $t + \Delta t$ can be determined from the following equation:

$$\vec{r}_{t+\Delta t}(P) = \vec{r}_t(P) + \vec{u}_t(P)\Delta t \tag{16}$$

The velocities of the control volumes are also updated. The velocity of the site at a time $t + \Delta t$ is determined from integration of Eqn. 14. The right-hand side gives the total force on the site, so the velocity is given by finite-differencing of Eqn. 14:

$$\vec{u}_{t+\Delta t}(P) = \frac{(\rho V)_t}{(\rho V)_{t+\Delta t}}\vec{u}_t(P) + \frac{1}{(\rho V)_{t+\Delta t}}\vec{F}_t(P)\Delta t \tag{16}$$

Here, $\vec{F}_t(P)$ is the resultant force on point ***P*** found from Eqn. 14.

D. Boundary Conditions

The erosion model must be coupled to a flow field solver that provides boundary conditions for the conservation equations. The flow field solver will be run for a macro time step. Gas shear and pressure forces, heat transfer, and other necessary values are used as input for the erosion model. The erosion model is then run between macro time steps. Note that this MSD model does not explicitly alter the gas properties at the surface of the nozzle wall and has a prescribed composition and state at the surface. The output from the erosion model, i.e. composition and mass injected into the flow and wall geometry, is used as input for the next macro time step of the flow field solver. Fully coupled simulations will require linking both approaches so that the boundary conditions are automatic, local, and fully matched. This couple to a flow field solver is one of the future goals of this study.

III. Results and Discussion

The erosion code is also applied to several situations representing solid propellant combustion. The first case is pure ammonium perchlorate (AP) with a nonuniform temperature profile prescribed at the surface of the solid. The second case is an ammonium perchlorate/polybutadiene binder (AP-binder) sandwich configuration with a uniform temperature profile prescribed at the surface of the solid propellant. The final case is an AP-binder sandwich with a nonuniform temperature profile prescribed at the surface of the solid propellant. Both sandwiches are three layer

sandwiches with AP being the outer layers and binder being the inner layer. These cases demonstrate the ability of this approach to model an arbitrary temperature profile applied to a heterogeneous composition.

The simulation domain is 600 μm by 600 μm. The grid is composed of 101 nodes in the axial direction and 80 nodes in the radial direction. This number of grid nodes is close to the minimum number sufficient to produce grid independent erosion results, i.e. the erosion depth does not change if the resolution of the grid is increased in either direction. Fewer nodes are required in the radial direction due to the boundary conditions. The total simulation time is 120 ms, corresponding to the time scales at which erosion can occur. The simulation time step is 0.02 ms. The limiting factor on the time step is stability of the solver. At the beginning of the simulation the material is uniformly at 300 K. For cases 1 and 3 the temperature profile applied at the top eroded surface is a quadratic profile with minimums at both top domain edges of 720 K and a maximum in the middle of the top edge of 820 K. For case 2 the temperature at the top eroded surface is uniformly at 820 K. The bottom boundary is isothermal at 300 K and the left and right surfaces are adiabatic. For case 1 the material is uniformly AP. For cases 2 and 3 the materials are AP on the outer layers of the sandwich with thicknesses of 275 μm each and the inner layer of the sandwich is polybutadiene binder with a thickness of 50 μm. The properties used for AP are a density (ρ) of 1760.0 kg/m^3, thermal conductivity (k) of 0.4114 W/m/K, specific heat capacity (c_p) of 1593.6 J/kg/K, and melting temperature (T_M) of 825.0 K.[23,24] For the polybutadiene binder the properties used are a density (ρ) of 880.0 kg/m^3, thermal conductivity (k) of 0.2148 W/m/K, specific heat capacity (c_p) of 3048.5 J/kg/K, and melting temperature (T_M) of 825.0 K. The reactions used in the simulation consist of the decomposition of AP with Arrhenius reaction rate parameters $A = 5.0 \cdot 10^6$ kg/m^2/s, $\eta = 0.0$, and $E_A = 92{,}109.6$ J/mol and the decomposition of the polybutadiene binder with Arrhenius reaction rate parameters $A = 2.6 \cdot 106$ kg/m^2/s, $\eta = 0.0$, and $E_A = 288{,}052$ J/mol.

Figures 4 through 6 show the results of the three cases with four different times shown for each case. The maximum erosion depths for each layer and each time are summarized in Table I. Note that all these cases did NOT include coupling to gas phase and therefore, only the surface regression effect has been simulated. The results report below are therefore, not typical of a full AP+binder combustion. However, the ability of the current model to capture surface motion is demonstrated.

Table I. Maximum erosion depth for layers in solid propellant combustion.

Case, layer	Maximum erosion depth at specified time			
	30 ms	60 ms	90 ms	120 ms
1, AP erosion depth	0.110 mm	0.224 mm	0.338 mm	0.452 mm
2, AP erosion depth	0.110 mm	0.224 mm	0.338 mm	0.452 mm
2, Binder erosion depth	~0.0 μm	~0.0 μm	3.8 μm	11.4 μm
3, AP erosion depth	0.110 mm	0.224 mm	0.338 mm	0.444 mm
3, Binder erosion depth	~0.0 μm	~0.0 μm	3.8 μm	11.4 μm

Figure 4 corresponds to case 1, the pure AP with a nonuniform temperature distribution. It is apparent that the ammonium perchlorate is eroded much faster at the center with a higher maximum temperature of 820 K than at the edges both with temperatures of 720 K. Because of the exponential dependence in the pyrolysis rates on temperature, the center is eroded 2.5 times the edge erosion despite the only 100 K temperature difference. Also apparent is the shallow heat penetration depth. The heat does not penetrate very deeply into the AP before the material is eroded. Figure 5 corresponds to case 2, the AP-binder sandwich with a uniform applied temperature of 820 K. Because of the much higher pyrolysis rate of AP, the middle layer of binder becomes quickly exposed. This binder is then eroded not only from the top, but also the sides leading to an increased rate of release of the binder. Once coupled to the flow solver, this unsteady mass release into the flow should greatly affect the boundary layer. Note that despite the small layer of binder in the middle the AP reaches the same maximum erosion depth as the first case, because of the uniformly applied temperature. The binder maximum erosion depth is 40 times less than the AP at the end of the simulation. Figure 6 corresponds to case 3, the AP-binder sandwich with the nonuniform temperature profile from case 1. The combination of results from cases 1 and 2 are apparent. The AP is eroded quickly and the binder layer is then eroded from all sides.

The binder is seen to require more energy for pyrolysis than the AP and therefore it erodes an order of magnitude slower. The response of the material does not match experimental expectations. The erosion model is not currently coupled to a flow solver, and as such the regression of the surface does not affect the imposed boundary conditions. However, the capability of the code to model an arbitrary composition and applied temperature profile with desired reaction mechanism has been demonstrated through these simulations.

Finally the three-dimensional capabilities of the model are applied to a simple three-dimensional situation involving particle impacts. Specifically, two particles are impacted simultaneously onto a three-dimensional wall 1

mm by 1 mm in exposed area and 0.25 mm deep. The grid used to simulate the wall is 20 nodes by 20 nodes on the impacting surface and 10 nodes deep. The nozzle wall material is carbon material with properties as given previously. The two impacting particles were 125 μm aluminum cubes modeled with 5 nodes in each direction giving 25 nodes per particle with properties as given previously. The particles were travelling at 100 m/s towards the wall. Simulation time was long enough for the particles to break apart and rebound from the impact, about 1 ms.

The results of the three-dimensional particle impact simulations are found in Fig. 7. A series of diagrams from the simulation are given to provide an idea of the three-dimensional impact results over time. Figure 9a begins at the exact time of the first particle impact. Breakup of the particle occurs within the first 0.02 ms of the simulation. At 0.06 ms the particle impact has produced visible lifted edges around the impact crater. At the end of the simulation a crater with a depression twice the size of the impacting particle is present. The radius of effect of the particle impact is four times the size of the particle. These simulations show impact cratering matching expectations providing evidence of the validity of the model being used.

IV. Conclusion

The primary objective of the study is to develop a comprehensive model that can simulate the erosion process in a rocket nozzle, predict erosion rates and paths for future, high pressure nozzles, and allow a greater understanding so that erosion mitigation methods can be developed. The primary aspects of erosion to be completed were determined to be surface forces, particle impacts, heat transfer, chemical kinetics, and surface melting. A MSD node centered, finite-volume model formulation was extended from being having only particle impact effects, to also include shear and pressure forces, heat transfer, and chemical kinetics. Additionally, the model has is quite robust with a rheological model that allows realistic materials to be simulated with true equations of state. This model can simulate not only nozzle erosion, but also burning of the solid fuel and shockwave propagation through the solids.

Erosion studies were also performed on a realistic propellant consisting of either pure ammonium perchlorate or an ammonium perchlorate/polybutadiene binder sandwich with uniform and nonuniform applied temperature profiles. Although the propellant was not eroded in a way consistent with experiments, the power of the erosion module was demonstrated.

Preliminary studies of three-dimensional impacts have also been performed. It has been seen that the model in its three-dimensional form agrees qualitatively with expectations. Particle impacts resulted in a crater formation, as has been seen in particle impact experiments. Simultaneous particle impacts were also demonstrated. The next simulations will include other, already considered aspects of the erosion process, such as chemistry, in the three-dimensional simulations providing more validation.

Future plans will include developing a more reliable use of processor resources. With the current parallel design processors are chosen and allocated at the start of model run time, load imbalances between processors can develop as the nozzle material is eroded. In order to fully utilize processor resources, a method for dynamically assign calculations and nodes to different processors may be investigated. The surface kinetics of tungsten-rhenium will be ascertained so that erosion studies can be performed that include all erosive effects on multiple real-world nozzle materials. Additionally, if liquid melt layer effects are determined to be important, they will be added to the erosion model. The model is also currently being coupled to a large-eddy simulation flow solver. Through this coupling, validation of the erosion model can continue as high fidelity simulations of a rocket nozzle firing and its subsequent erosion can be performed. After these simulations are validated, parametric studies of erosions can be completed, the relative importance of the aspects of erosion can be determined, and effective erosion mitigation techniques can be developed.

Appendix

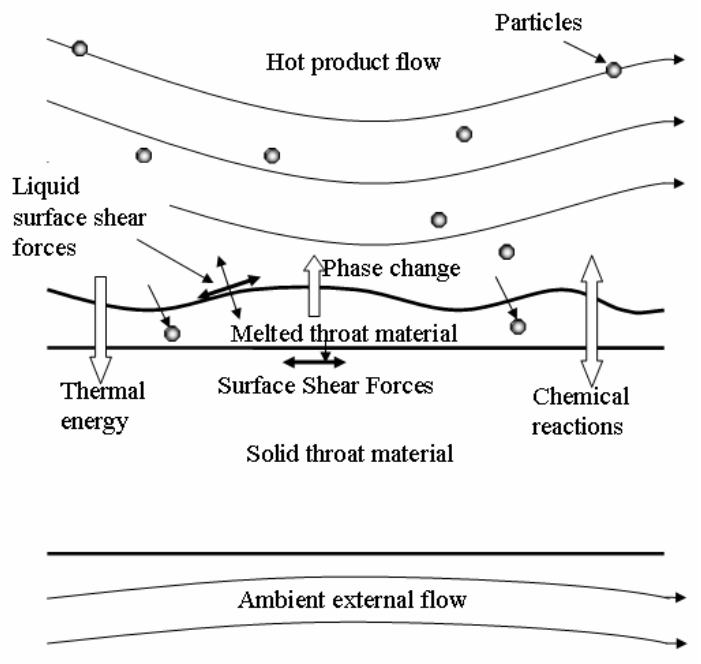

Figure 1. Physical processes affecting erosion.

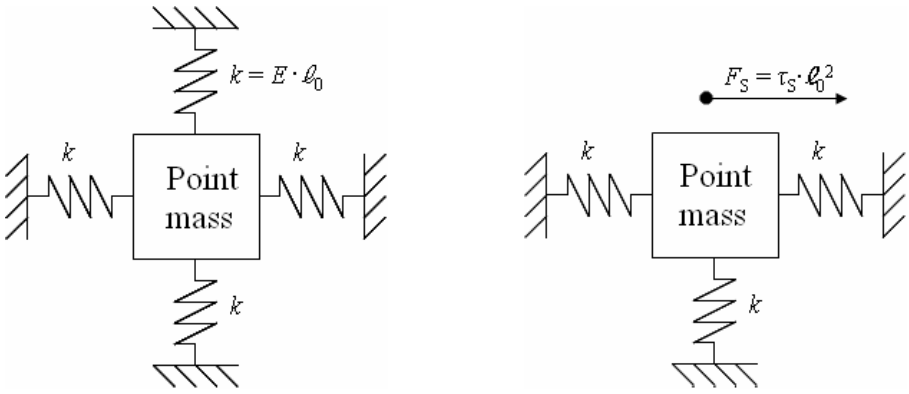

(a) Interior site **(b) Exposed site**

Figure 2. Lattice site for MSD model.

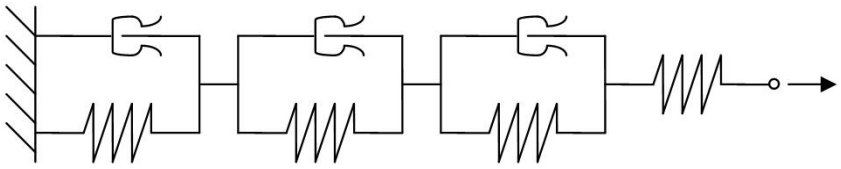

Figure 3. Rheological model for elastic and multiple plastic regimes.

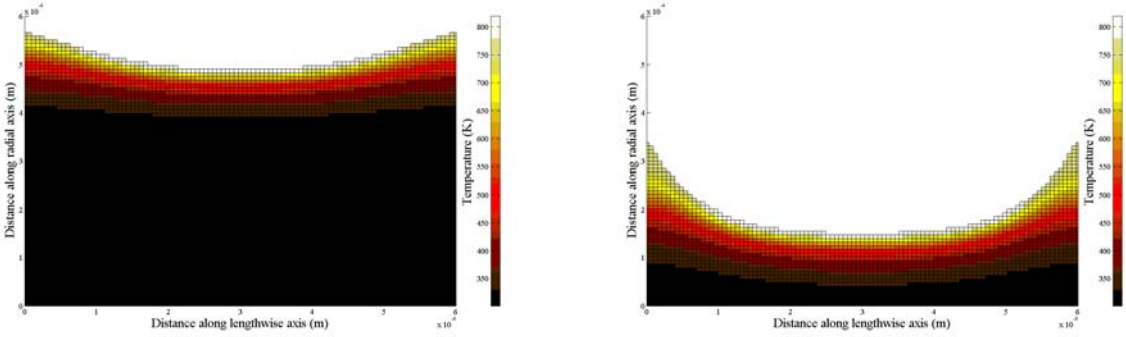

(a) At 30 ms. **(b) At 120 ms.**

Figure 4. Results for case 1 simulations at various times.

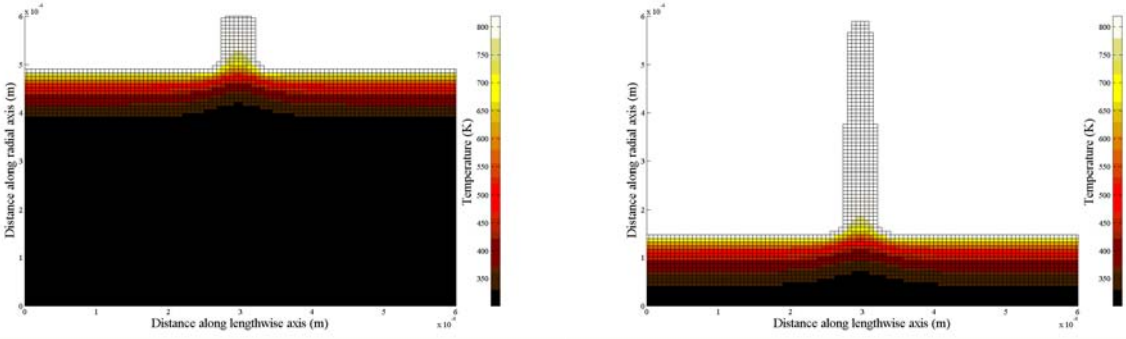

(a) At 30 ms. **(b) At 120 ms.**

Figure 5: Results for case 2 simulations at various times.

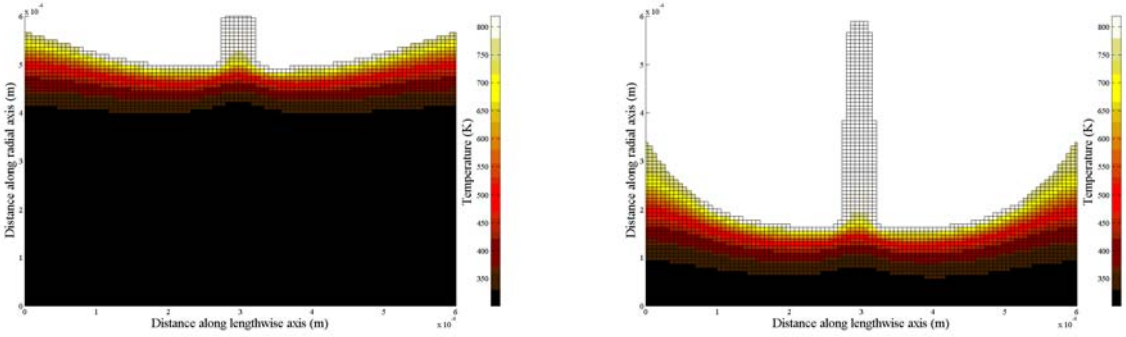

(a) At 30 ms. **(b) At 120 ms.**

Figure 6: Results for case 3 simulations at various times.

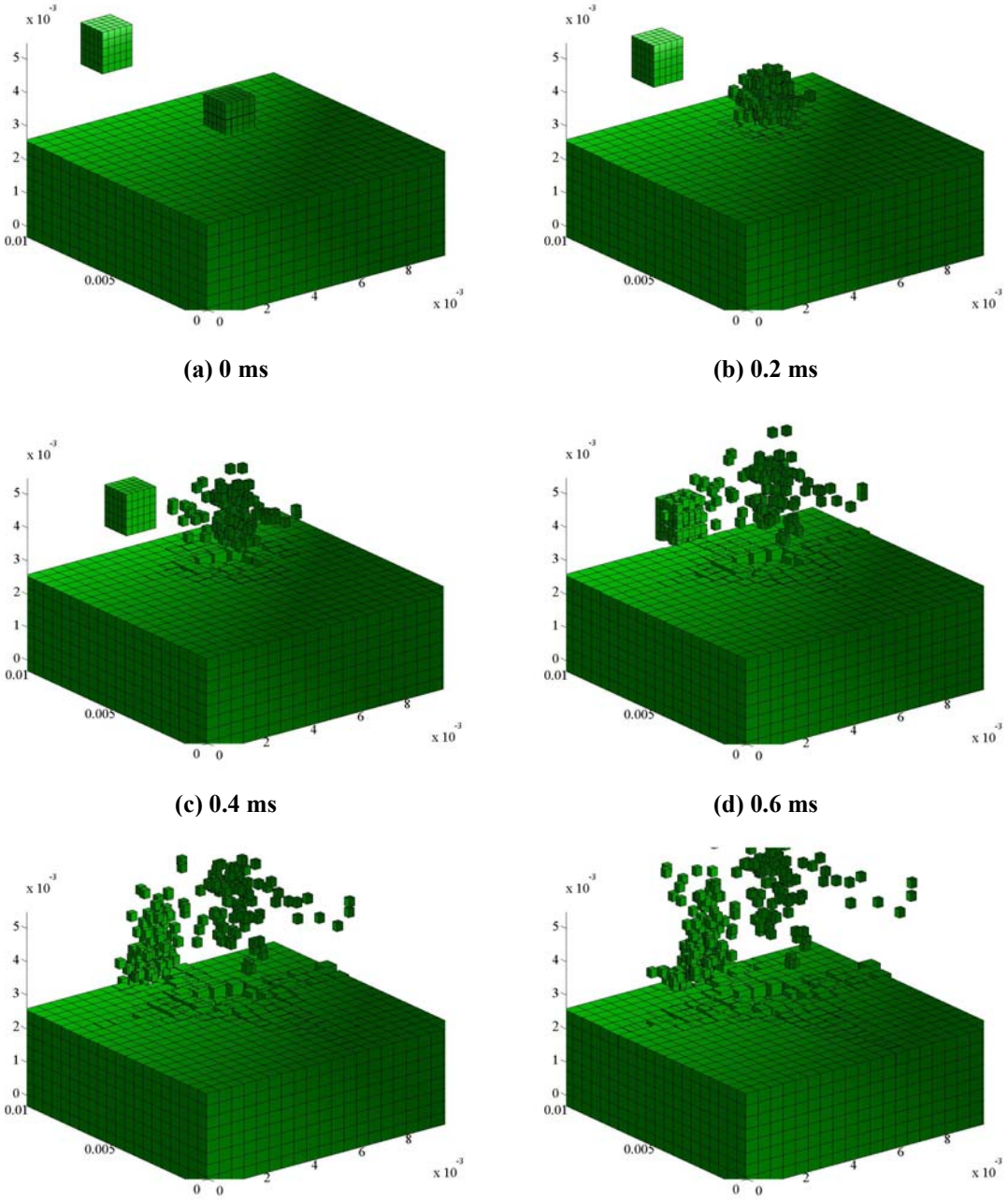

(a) 0 ms **(b) 0.2 ms**

(c) 0.4 ms **(d) 0.6 ms**

(e) 0.8 ms **(f) 1.0 ms**

Figure 7. Simulation of simultaneous two particle impact with three-dimensional wall.

Acknowledgments

This work was funded by a subcontract from Penn State University under an Office of Naval Research (Dr. Judah Goldwasser, Program Manager) MURI on "Fundamental Understanding of Propellant/Nozzle Interaction for Rocket Nozzle Erosion Minimization under very High Pressure Conditions".

References

[1]Hanagud, Sathya V., Wilkinson, Angus, Menon, Suresh, & Seitzman, Jerry, "Annual Report: Mechanisms of time dependent nozzle erosion processes," written for the Office of Naval Research, Arlington, VA, 2005.

[2]Sutton, George P., & Biblarz, Oscar, Rocket Propulsion Elements, 7th ed., John Wiley & Sons, Inc. (2001), 605 Third Avenue, New York, NY 10158-0012.

[3]Sopok., S., Rickard, C., & Dunn, S., "Thermal-chemical-mechanical gun bore erosion of an advanced artillery system part two: modeling and predictions," WEAR, Vol. 258, 2005, p 671-683.

[4]Sopok, S., O'Hara, P., & Pflegl, G., "Unified Computer Model for Predicting Thermochemical Erosion in Gun Barrels," *Journal of Propulsion and Power*, Vol. 15, No. 4, July-August 1999, p 601-612.

[5]Niu, Yang-Yao, & Tsai, Chih-Shung, "Numerical Modeling of Erosion on the Metallic Surface by the Dilute Particulate Flow Impact," AIAA Paper 99-3761, 30th AIAA Fluid Dynamics Conference, Norfolk, VA, 1999

[6]Niu, Y., & Tsai, C., "Simulation of erosion by the dilute particle flow impact," *Numerical Heat Transfer*, Part A, Vol. 37, 2000, p 167-187.

[7]Wirzberger, H. and Yaniv, S., "Prediction of erosion in a solid rocket motor by alumina particles," 41st AIAA/ASME/ASEE Joint Propulsion Conference & Exhibit, 10-13 July, 2005, AIAA 2005-4496

[8]Palaninathan, R. & Bindu, S., "Modeling of Mechanical Ablation in Thermal Protection Systems," Journal of Spacecraft and Rockets, Vol. 42, No. 6, November-December 2005, p 971-979.

[9]Siddiqui, A. O., & Balasubrahmanyam, G., "Design of Ablative Liners for High Heat and Erosive Conditions," *Journal of Reinforced Plastics and Composites*, Vol. 24, No. 9, 2005, p 993-1007.

[10]Li, D.Y., Elalem, K., Anderson, M.J., & Chiovelli, S., "A microscale dynamical model for wear simulation," *WEAR*, Vol. 225-229, 1999, p 380-386.

[11]Elalem, K., & Li, D.Y., "Dynamical simulation of an abrasive wear process," *Journal of Computer-Aided Materials Design*, Vol. 6, 1999, p 185-193.

[12]Chen, Q., & Li, D.Y., "Computer simulation of solid particle erosion," *WEAR*, Vol. 254, 2003, p 203-210.

[13]Chen, Q., & Li, D.Y., "Computer simulation of solid-particle erosion of composite materials," *WEAR*, Vol. 255, 2003, p 78-84.

[14]Liggett, Nicholas and Menon, Suresh, "Simulation of Nozzle Erosion Process," Office of Naval Research, Arlington, VA, 2006.

[15]Snih, T. M., Numerical Heat Transfer, Hemisphere Publishing Corporation (1984), New York, NY.

[16]Tannehill, J., Anderson, D., & Pletcher, R., Computational Fluid Mechanics and Heat Transfer, 2nd ed., Taylor & Francis (1997), Philadelphia, PA 19106.

[17]Kuo, Kenneth K., Principles of Combustion, John Wiley & Sons, Inc. (1986), New York, NY

[18]Kuo, Kenneth K., & Keswani, S. T., "A Comprehensive Theoretical Model for Carbon-Carbon Composite Nozzle Recession," *Combustion Science and Technology*, Vol. 42, 1985, p 145-164.

[19]Coltrin, M.E., Kee, R.J., & Rupley, F.M., "Surface Chemkin: A general formalism and software for analyzing heterogeneous chemical kinetics at a gas-surface interface," *International Journal of Chemical Kinetics*, Vol. 23, 1991, p 1111-1128.

[20]Coltrin, M.E., Kee, R.J., & Rupley, F.M., "Surface Chemkin: A fortran package for analyzing heterogeneous chemical kinetics at a solid surface - gas phase interface," Sandia Report SAND90-8003B, July 1991.

[21]Coltrin, M.E., Kee, R.J., & Rupley, F.M., "Surface Chemkin III: User manual," *Reaction Design*, 1996.

[22]Porumbel, I. and Menon, S., "Large-Eddy Simulation of Bluff Body Stabilized Premixed Flames," AIAA-2006-0152, 44th AIAA Aerospace Sciences Meeting, Reno, NV, January, 2006.

[23]Surzhikov, S. T., & Krier, H., "Quasi-One-Dimensional Model of Combustion of Sandwich Heterogeneous Propellant," *High Temperature Mass Transfer and Physical Gas Dynamics*, Vol. 39, No. 4, 2001, p 586-595.

[24]Massa, L., Jackson, T. L., & Buckmaster, J., "New Kinetics for a Model of Heterogeneous Propellant Combustion," *Journal of Propulsion and Power*, Vol. 21, No. 5, September-October 2005, p 914-924

[25]Powers, David L., Boundary Value Problems, 4th ed., Academic Press (1999), 200 Wheeler Road, Bulington, MA 01803, USA

[26]Kuo, K.., Evans, B., Acharya, R., Favorito, N., Ferrara, P., Moore, J., & Boyd, E., "Annual Progress Report for MURI 12 Rocket Nozzle Erosion Minimization (RNEM)," written for the Office of Naval Research, Arlington, VA, 2005.

[27]Yang, Vigor, & Thakre, Piyush, "Annual Report (2004/2005) Modeling and Simulation of Nozzle Material Erosion," written for the Office of Naval Research, Arlington, VA, 2005.

[28]Avallone, Eugene A. & Baumeister III, Theodore, Marks' Standard Handbook for Mechanical Engineers, 10th ed., The McGraw-Hill Companies, Inc. (1996), New York, NY.

[29]Lee, Tae-Ho, "Experimental Study of the Nozzle Surface Regression Rate to the Heat Transfer," *Journal of Propulsion and Power*, Vol. 22, No. 1, January-February 2006, p 221-223.

[30]Gowariker, V. R., "Mechanical and Chemical Contributions of the Erosion Rates of Graphite Throats in Rocket Motor Nozles," *Journal of Spacecraft and Rockets*, Vol. 3, No. 10, October 1966, p 1490-1494.

[31]Gates, A. M, "In situ measurements of carbon dioxide, 0.37–4.0 μm particles, and water vapor in the stratospheric plumes of small rockets," *Journal of Geophysical Research* (2002), Vol. 107, No. D22, p AAC8-1-10.